Research Article

Practical Gammatone-Like Filters for Auditory Processing

A. G. Katsiamis,[1] E. M. Drakakis,[1] and R. F. Lyon[2]

[1] *Department of Bioengineering, The Sir Leon Bagrit Centre, Imperial College London, South Kensington Campus, London SW7 2AZ, UK*

[2] *Google Inc., 1600 Amphitheatre Parkway Mountain View, CA 94043, USA*

This paper deals with continuous-time filter transfer functions that resemble tuning curves at particular set of places on the basilar membrane of the biological cochlea and that are suitable for practical VLSI implementations. The resulting filters can be used in a filterbank architecture to realize cochlea implants or auditory processors of increased biorealism. To put the reader into context, the paper starts with a short review on the gammatone filter and then exposes two of its variants, namely, the differentiated all-pole gammatone filter (DAPGF) and one-zero gammatone filter (OZGF), filter responses that provide a robust foundation for modeling cochlea transfer functions. The DAPGF and OZGF responses are attractive because they exhibit certain characteristics suitable for modeling a variety of auditory data: level-dependent gain, linear tail for frequencies well below the center frequency, asymmetry, and so forth. In addition, their form suggests their implementation by means of cascades of N identical two-pole systems which render them as excellent candidates for efficient analog or digital VLSI realizations. We provide results that shed light on their characteristics and attributes and which can also serve as "design curves" for fitting these responses to frequency-domain physiological data. The DAPGF and OZGF responses are essentially a "missing link" between physiological, electrical, and mechanical models for auditory filtering.

1. INTRODUCTION

For more than twenty years, the VLSI community has been performing extensive research to comprehend, model, and design in silicon naturally encountered biological auditory systems and more specifically the inner ear or cochlea. This ongoing effort aims not only at the implementation of the ultimate artificial auditory processor (or implant), but also to aid our understanding of the underlying engineering principles that nature has applied through years of evolution. Furthermore, parts of the engineering community believe that mimicking certain biological systems at architectural and/or operational level should in principle yield systems that share nature's power-efficient computational ability [1]. Of course, engineers bearing in mind what can be practically realized must identify what should and what should not be blindly replicated in such a "bioinspired" artificial system. Just as it does not make sense to create flapping airplane wings only to mimic birds' flying, it seems equally meaningful to argue that not all operations of a cochlea can or should be replicated in silicon in an exact manner. Abstractive operational or architectural simplifications dictated by logic and the available

technology have been crucial for the successful implementation of useful hearing-type machines.

A cochlea processor can be designed in accordance with two well-understood and extensively analyzed architectures: the parallel filterbank and the traveling-wave filter cascade. A multitude of characteristic examples representative of both architectures have been reported [2–6]. Both architectures essentially perform the same task; they analyze the incoming spectrum by splitting the input (audio) signal into subsequent frequency bands exactly as done by the biological cochlea. Moreover, transduction, nonlinear compression, and amplification can be incorporated in both to model effectively inner- and outer-hair-cells (IHC and OHC, resp.) operation yielding responses similar to the ones observed from the biological cochleae. Figure 1 illustrates how basilar membrane (BM) filtering is modeled in both architectures.

2. MOTIVATION: ANALOG VERSUS DIGITAL

Hearing is a perceptive task and nature has developed an efficient strategy in accomplishing it: *the adaptive traveling-wave*

amplifier structure. Bioinspired analog circuitry is capable of mimicking the dynamics of the biological prototype with ultra-low power consumption in the order of tens of μWs (comparable to the consumption of the biological cochlea). Comparative calculations would show that opting for a custom digital implementation of the same dynamics would still cost us considerably more in terms of both silicon area and power consumption [7]; power consumption savings of at least two orders of magnitude and silicon area savings of at least three can be expected should ultra-low power analog circuitry be used effectively. This is due to the fact that in contrast to the power hungry digital approaches, where a single operation is performed out of a series of switched-on or -off transistors, the individual devices are treated as analog computational primitives; operational tasks are performed in a continuous-time analog way by direct exploitation of the physics of the elementary device. Hence, the energy per unit computation is lower and power efficiency is increased. However, for high-precision simulation, digital is certainly more energy-efficient [8].

Apart from that, realizing filter transfer functions in the digital domain does not impose severe constraints and trade-offs to the designer apart from stability issues. For example, in [9], a novel application of a filtering design technique that can be used to fit measured auditory tuning curves was proposed. Auditory filters were obtained by minimizing the squared difference, on a logarithmic scale, between the measured amplitude of the nerve tuning curve and the magnitude response of the digital IIR filter. Even though this approach will shed some light on the kind of filtering the real cochlea is performing, such computational techniques are not suited for analog realizations.

Moreover, different analog design synthesis techniques (switched-capacitor, Gm-C, log-domain, etc.) yield different practical implementations and impose different constraints on the designer. For example, it is well known that realizing finite transmission zeros in a filter's transfer function using the log-domain circuit technique is a challenging task [10].

As such, and with the filterbank architecture in mind, finding filter transfer functions that have the potential for an efficient analog implementation while grasping most of the biological cochlea's operational attributes is the focus of this and our ongoing work. It goes without saying that the design of these filters in digital hardware (or even software) will be a much simpler task than in analog.

3. COCHLEA NONLINEARITY: BM RESPONSES

The cochlea is known to be a nonlinear, causal, active system. It is active since it contains a battery (the difference in ionic concentration between scala vestibuli, tympani, and media, called the endocochlear potential, acts as a silent power supply for the hair cells in the organ of Corti) and nonlinear as evidenced by a multitude of physiological characteristics such as generating otoacoustic emissions.

In 1948, Thomas Gold (22 May 1920–1922 June 2004), a distinguished cosmologist, geophysicist, and original thinker with major contributions to theories of biophysics, the origin of the universe, the nature of pulsars, the physics of the mag-

netosphere, the extra terrestrial origins of life on earth, and much more, argued that there must be an active, undamping mechanism in the cochlea, and he proposed that the cochlea had the same positive feedback mechanism that radio engineers applied in the 1920s and 1930s to enhance the selectivity of radio receivers [11, 12]. Gold had done army-time work on radars and as such he applied his signal-processing knowledge to explain how the ear works. He knew that to preserve signal-to-noise ratio, a signal had to be amplified before the detector. "Surely nature cannot be as stupid as to go and put a nerve fiber—the detector—right at the front end of the sensitivity of the system," Gold said. Gold had his idea back in 1946, while being a graduate astrophysicist student at Cambridge University, England. He spotted a flaw in the classical theory of hearing (the sympathetic resonance model) developed by Hermann von Helmholtz [13] almost a century before. Helmholtz's theory assumed that the inner ear consists of a set of "strings," each of which vibrates at a different frequency. Gold, however, realized that friction would prevent resonance from building up and that some active process is needed to counteract the friction. He argued that the cochlea is "regenerative" adding energy to the very signal that it is trying to detect. Gold's theories also daringly challenged von Békésy's large-scale traveling-wave cochlea models [14] and he was also the first to predict and study otoacoustic emissions. Ignored for over 30 years, his research was rediscovered by a British engineer by the name of David Kemp, who in 1979 proposed the "active" cochlea model [15]. Kemp suggested that the cochlea's gain adaptation and sharp tuning were due to the OHC operation in the organ of Corti.

Early physiological experiments (Steinberg and Gardner 1937 [16]) showed that the loss of nonlinear compression in the cochlea leads to loudness recruitment.[1] Moreover, it can be shown that the dynamic range of IHC (the cochlea's transducers) is about 60 dB rendering them inadequate to process the achieved 120 dB of input dynamic range without signal compression. It is by now widely accepted that the 6 orders of magnitude of input acoustic dynamic range supported by the human ear are due to OHC-mediated compression.

Evidence for the cochlea nonlinearity was first given by Rhode. In his papers [17, 18], he demonstrated BM measurements yielding cochlea transfer functions for different input sound intensities. He observed that the BM displacement (or velocity) varied highly nonlinearly with input level. More specifically, for every four dBs of input sound pressure level (SPL) increase, the BM displacement (or velocity) as measured at a specific BM place changed only by one dB. This compressive nonlinearity was frequency-dependent and took place only near the most sensitive frequency region, the peak of the tuning curve. For other frequencies, the system behaved linearly; that is, one dB change in input SPL yielded one dB of output change for frequencies away from the center frequency. In addition, for high input SPL, the

---

[1] Loudness recruitment occurs in some ears that have high-frequency hearing loss due to a diseased or damaged cochlea. Recruitment is the rapid growth of loudness of certain sounds that are near the same frequency of a person's hearing loss.
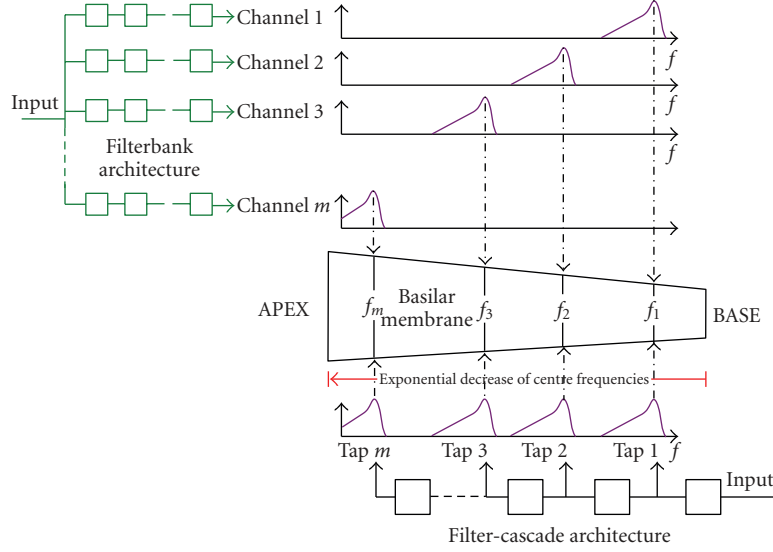
FIGURE 1: Graphical representation of the filterbank and filter-cascade architectures. The filters in the filter-cascade architecture have non-coincident poles; their cut-off frequencies are spaced-out in an exponentially decreasing fashion from high to low. On the other hand, the filter cascades per channel of the filterbank architecture have identical poles. However, each channel follows the same frequency distribution as in the filter-cascade case.

high-frequency roll-off slope broadened (the selectivity decreased) with a shift of the peak towards lower frequencies, in contrast to low input intensities where it became steeper (the selectivity increased) with a shift of the peak towards higher frequencies. Figure 2 illustrates these results.

From the engineering point of view, we seek filters whose transfer functions can be controlled in a similar manner, that is,

(i) low input intensity → high gain and selectivity and shift of the peak to the "right" in the frequency domain;

(ii) high input intensity → low gain and selectivity and shift of the peak to the "left" in the frequency domain.

As a first rough approximation of the above behavior, it is worth noting that the simplest VLSI-compatible resonant structure, the lowpass biquadratic filter (LP biquad), gives a frequency response that exhibits this kind of level-dependent compressive behavior by varying only one parameter, its quality factor. The standard LP biquad transfer function is

$$H_{\mathrm{LP}}(s) = \frac{\omega_o^2}{s^2 + (\omega_o/Q)s + \omega_o^2}, \tag{1}$$

where ω_o is the natural (or pole) frequency and Q is the quality factor. The frequency, where the peak gain occurs or center frequency (CF) is related to the natural frequency and Q, is as follows:

$$\omega_{\mathrm{CF}}^{\mathrm{LP}} = \omega_o\sqrt{1 - \frac{1}{2Q^2}}, \tag{2}$$
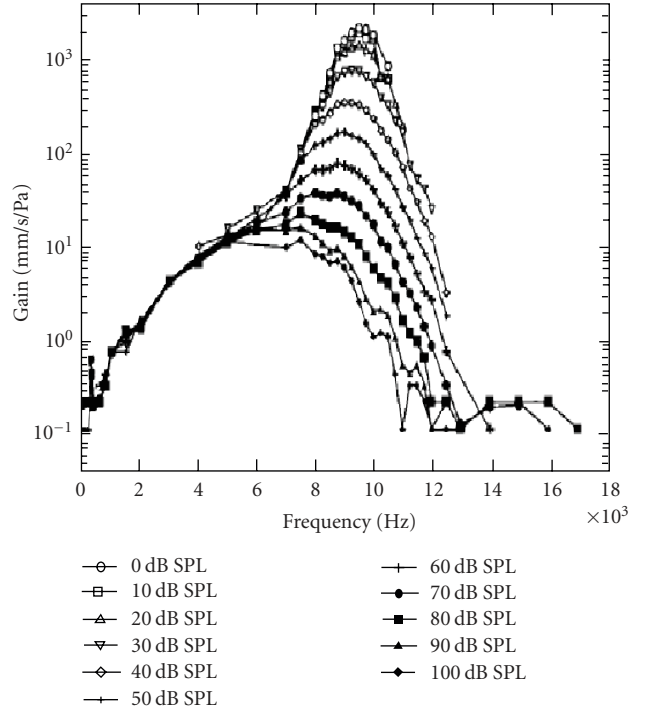

FIGURE 2: Frequency-dependent nonlinearity in BM tuning curves, adapted from Ruggero et al. [19].

suggesting the lowest Q value of $1/\sqrt{2}$ for zero CF. The LP biquad peak gain can be parameterized in terms of Q according to

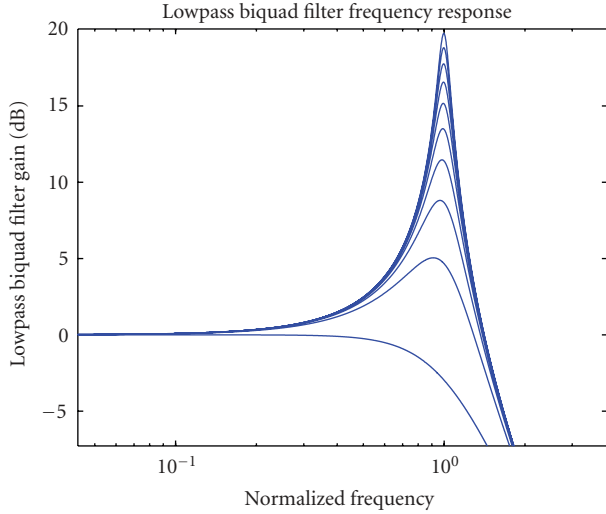$$H_{\mathrm{LP}_{\max}} = \frac{Q}{\sqrt{1 - 1/4Q^2}}. \tag{3}$$

FIGURE 3: The LP biquad transfer function illustrating level-dependent gain with single parameter variation. The dotted line shows roughly how the peak shifts to the right as gain increases. The frequency axis is normalized to the natural frequency.

Figure 3 shows a plot of the LP biquad transfer function with Q varying from $1/\sqrt{2}$ to 10. Observe that as Q increases, ω_{CF}^{LP} tends to be closer to ω_o modeling the shift of the peak towards high frequencies as intensity decreases.

4. REFERENCE MEASURES OF BM RESPONSES

With such a plethora of physiological measurements (not only from various animals but also from several experimental methods), it is practically impossible to have universal and exquisitely insensitive measures which define cochlea biomimicry and act as "reference points." In other words, it seems that we do not have an absolute BM measurement against which all the responses from our artificial systems could be compared. Eventually, a biomimetic design will be the one which will have the potential to achieve performances of the same order of magnitude to those obtained from the biological counterparts. The goal is not necessarily the faithful reproduction of every feature of the physiological measurement, but just of the right ones. Of course, the right features are not known in advance; so there must be an active collaboration between the design engineers, the cochlea biophysicists, and those who treat and test the beneficiaries of the engineering efforts. To aid our discussion, we resort to Rhode's BM response measure defined in [20].

Rhode observed that the cochlea transfer function at a particular place in the BM is neither purely lowpass nor purely bandpass. It is rather an asymmetric bandpass function of frequency. He thus defined a graph, such as the one shown in Figure 4, where all tuning curves can be fitted by straight lines on log-log coordinates. The slopes (*S1, S2,* and *S3*), as well as the break points (ω_Z and ω_{CF}) defined as the locations where the straight lines cross, characterize a given response. Table 1, adapted from Allen [21] and extended
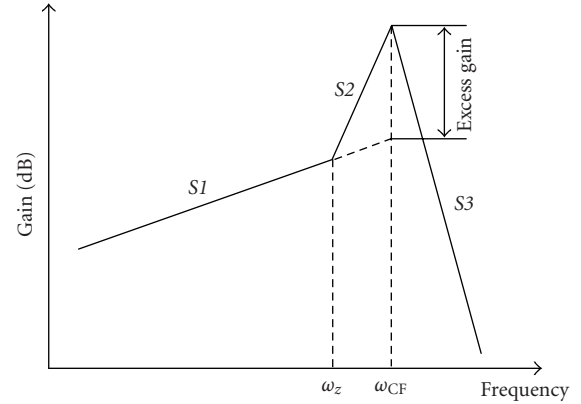

FIGURE 4: Rhode's BM frequency response measure, a piecewise approximation of the BM frequency response.

here, gives a summary of this parametric representation of BM responses from various sources.

Observe that ω_Z usually ranges between 0.5 and 1 octave below ω_{CF}, the slopes *S1* and *S2* range between 6 and 12 dB/oct and 20 and 60 dB/oct, respectively, and *S3* is lower than at least -100 dB/oct. In other words, it seems that *S1* corresponds to a first- or second-order highpass frequency shaping LTI network, *S2* to at least a fourth- (up to tenth-) order one, and *S3* to at least a seventeenth-order lowpass response. The minimum excess gain of $\sim$18 dB corresponds approximately to the peak gain of an LP biquad response with a Q value of 10.

Other BM measures, more insensitive to many important details and also more prone to experimental errors, are the Q_{10} (or Q_3) defined as the ratio of CF over the 10 dB or 3 dB bandwidth, respectively, and the "tip-to-tail ratio" relative to a low-frequency tail taken about an octave below the CF. Table 1 provides a good idea of what should be mimicked in an artificial/engineered cochlea. Filter transfer functions, which

   (i) can be tuned to have parameter values similar/comparable to the ones presented in Table 1,

  (ii) are gain-adjustable by varying as few parameters as possible (ideally one parameter),

 (iii) are suited in terms of practical complexity for VLSI implementation,

are what we ultimately seek to incorporate in an artificial VLSI cochlea architecture. In the following sections, a general class of such transfer functions is introduced and their properties are studied in detail.

5. THE GAMMATONE AUDITORY FILTERS

The gammatone (or Γ-tone) filter (GTF) was introduced by Johannesma in 1972 to describe cochlea nucleus response [25]. A few years later, de Boer and de Jongh developed the gammatone filter to characterize physiological data gathered from reverse-correlation (Revcor) techniques from primary auditory fibers in the cat [26, 27].

TABLE 1: Parametric representation of BM responses from various sources.

Data type	Reference	$\log_2(f_z/f_{Cf})$ (oct)	$S1$(dB/oct)	Max($S2$) (dB/oct)	Max($S3$) (dB/oct)	Excess gain (dB)	Conditions	
							Input SPL (dB)	f_{CF} (kHz)
BM	[17]	—	6	20	−100	28	80	7
BM	[20]	0.57	9	86	−288	27	50–105	7.4
BM	[22]	0.88	10	28	−101	17.4	20–100	15
BM	[23]	0.73	12	48.9	−110	32.5	10–90	10
BM	[23]	0.44	8	53.9	−286	35.9	0–100	9.5
Neural	[24]	0.5–0.8	0–10	50–170	< −300	50–80	—	>3

TABLE 2: Gammatone filter variants' transfer functions.

Filter type	Transfer function	
GTF	$H_{GTF}(s) = \dfrac{e^{j\varphi}\left[s + \omega_o/2Q + j\omega_o\sqrt{1 - 1/4Q^2}\right]^N + e^{-j\varphi}\left[s + \omega_o/2Q - j\omega_o\sqrt{1 - 1/4Q^2}\right]^N}{\left[s^2 + (\omega_o/Q)s + \omega_o^2\right]^N}$	(4)
APGF	$H_{APGF}(s) = \dfrac{K}{\left[s^2 + (\omega_o/Q)s + \omega_o^2\right]^N}, \quad K = \omega_o^{2N}$ for unity gain at DC	(5)
DAPGF	$H_{DAPGF}(s) = \dfrac{Ks}{\left[s^2 + (\omega_o/Q)s + \omega_o^2\right]^N}, \quad K = \omega_o^{2N-1}$ for dimensional consistency	(6)
OZGF	$H_{OZGF}(s) = \dfrac{K(s + \omega_z)}{\left[s^2 + (\omega_o/Q)s + \omega_o^2\right]^N}, \quad K = \omega_o^{2N-1}$ for dimensional consistency	(7)

However, Flanagan was the first to use it as a BM model in [28], but he neither formulated nor introduced the name "gammatone" even though it seems he had understood its key properties. Its name was given by Aertsen and Johannesma in [29] after observing the nature of its impulse response. Since then, it has been adopted as the basis of a number of successful auditory modeling efforts [30–33]. Three factors account for the success and popularity of the GTF in the audio engineering/speech-recognition community:

(i) it provides an appropriately shaped "pseudoresonant" [34] frequency transfer function making it easy to match reasonably well-measured responses;
(ii) it has a very simple description in terms of its time-domain impulse response (a gamma-distribution envelope times a sinusoidal tone);
(iii) it provides the possibility for an efficient hardware implementation.

The gammatone impulse response with its constituent components is shown in Figure 5. Note that for the gamma-distribution factor to be an actual probability distribution (i.e., to integrate to unity), the factor A needs to be $b^N/\Gamma(N)$, with the gamma function being defined for integers as the factorial of the next lower integer $\Gamma(N) = (N-1)!$. In practice, however, A is used as an arbitrary factor in the filter response and it is typically chosen to make the peak gain equal unity.
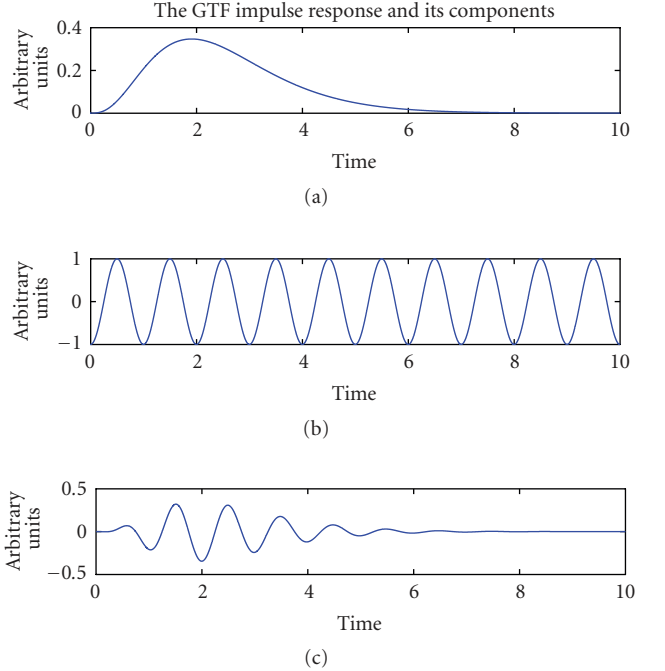
FIGURE 5: The components of a gammatone filter impulse response; the gamma-distribution envelope (top); the sinusoidal tone (middle); the gammatone impulse response (bottom).

$$
\begin{aligned}
\text{The gamma-distribution} \quad & At^{N-1}\exp(-bt) \\
\text{The tone} \quad & \cos(\omega_r t + \varphi) \\
\text{The gammatone} \quad & At^{N-1}e^{(-bt)}\cos(\omega_r t + \varphi)
\end{aligned} \tag{8}
$$

The parameters' order N (integer), ringing frequency ω_r (rad/s), starting phase φ (rad), and one-sided pole bandwidth b (rad/s), together with (8), complete the description of the GTF.

Three key limitations of the GTF are as follows.

(i) It is inherently nearly symmetric, while physiological measurements show a significant asymmetry in the auditory filter (see Section 6.5 for a more detailed description regarding asymmetry).

(ii) It has a very complex frequency-domain description (see (4)). Therefore, it is not easy to use parameterization techniques to realistically model level-dependent changes (gain control) in the auditory filter.

(iii) Due to its frequency-domain complexity, it is not easy to implement the GFT in the analog domain.

Lyon presented in [35] a close relative to the GTF, which he termed as all-pole gammatone filter (APGF) to highlight its similarity to and distinction from the GTF.

The APGF can be defined by discarding the zeros from a pole-zero decomposition of the GTF—all that remains is a complex conjugate pair of Nth-order poles (see (5)). The APGF was originally introduced by Slaney [36] as an "all-pole gammatone approximation," an efficient approximate implementation of the GTF, rather than as an important filter in its own right.

In this paper, we will expose the differentiated all-pole gammatone filter (DAPGF) and the one-zero gammatone filter (OZGF) as better approximations to the GTF, which inherits all the advantages of the APGF. It is worth noting that a third-order DAPGF was first used to model BM motion by Flanagan [28], as an alternative to the third-order GTF. The DAPGF is defined by multiplying the APGF with a differentiator transfer function to introduce a zero at DC (i.e., at $s = 0$ in the Laplace domain) (see (6)), whereas the OZGF has a zero anywhere on the real axis (i.e., $s = \alpha$ for any real value α) (see (7)).

The APGF, DAPGF, and OZGF have several properties that make them particularly attractive for applications in auditory modeling:

(i) they exhibit a realistic asymmetry in the frequency domain, providing a potentially better match to psychoacoustic data;

(ii) they have a simple parameterization;

(iii) with a single level-dependent parameter (their Q), they exhibit reasonable bandwidth and center frequency variation, while maintaining a linear low-frequency tail;

(iv) they are very efficiently implemented in hardware and particularly in analog VLSI;

(v) they provide a logical link to Lyon's neuromorphic and biomimetic traveling-wave filter-cascade architectures.

Table 2 summarizes GTF, APGF, DAPGF, and OZGF with their corresponding transfer functions.

6. OBSERVATIONS ON THE DAPGF RESPONSE

The DAPGF can be considered as a cascade of $(N - 1)$ identical LP biquads (i.e., an $(N - 1)$th-order APGF) and an appropriately scaled BP biquad. Therefore, the DAPGF is characterized as a complex conjugate pair of Nth-order pole locations with an additional zero location at DC. Unfortunately,
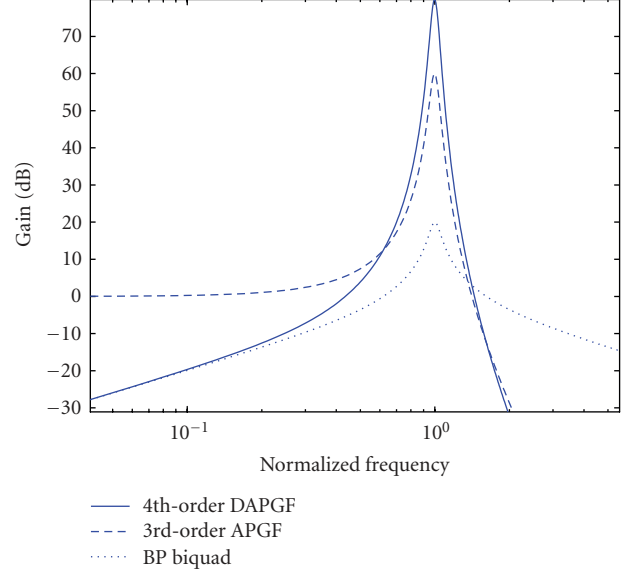

Figure 6: Transfer function of the DAPGF of $N = 4$ and $Q = 10$, its decomposition to a third-order APGF, and a scaled BP biquad with a gain of 20 dB. The frequency axis is normalized to the natural frequency.

this zero does not make the analytical description of the DAPGF as straightforward as in the case of the APGF (which is just an LP biquad raised to the Nth power). The DAPGF transfer function is

$$
\begin{aligned}
H_{\mathrm{DAPGF}}(s) &= \frac{K_1}{\left[s^2 + (\omega_o/Q)s + \omega_o^2\right]^{N-1}} \\
&\quad \times \frac{K_2 s}{s^2 + (\omega_o/Q)s + \omega_o^2} \\
&= \frac{K s}{\left[s^2 + (\omega_o/Q)s + \omega_o^2\right]^N} \\
&= \frac{\omega_o^{2N-1} s}{\left[s^2 + (\omega_o/Q)s + \omega_o^2\right]^N}.
\end{aligned}
\tag{9}
$$

Note that the constant gain term $K = K_1 K_2$ was chosen to be ω_o^{2N-1} in order to preserve dimensional consistency and aid implementation. Specifically, $K_1 = \omega_o^{2(N-1)}$ and $K_2 = \omega_o$.

Figure 6 illustrates that an Nth-order DAPGF, as defined previously, has both its peak gain and CF larger than its constituent $(N - 1)$th-order APGF. Its larger peak is due to the fact that the BP biquad is appropriately scaled (for 0 dB BP biquad gain; K_2 should be ω_o/Q, whereas here we set it to be ω_o) in order to maintain a constant gain across levels for the low-frequency tail as observed physiologically [17, 37]. In addition, since an Nth-order DAPGF consists of $(N - 1)$ cascaded LP biquads, it is reasonable to expect that the DAPGF will have a behavior closely related to the LP biquad's in terms of how its gain and selectivity change with varying Q values. Figure 7 illustrates this behavior.

Since the DAPGF can be characterized by two parameters only (N and Q), it would be very convenient to codify graphically how these parameters depend on each other and how their variation can achieve a given response that best fits
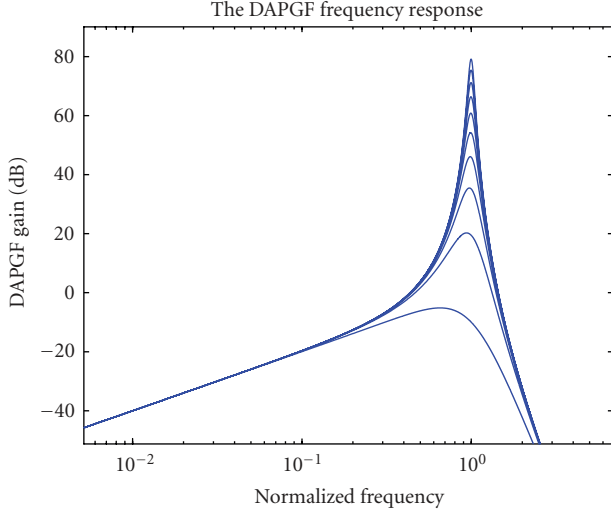
Figure 7: The DAPGF frequency response of $N = 4$ with Q ranging from 0.75 to 10. The frequency axis is normalized to the natural frequency.

physiological data. In the following sections, we derive expressions for the peak gain, CF, bandwidth, and low-side dispersion in an attempt to characterize the DAPGF response and create graphs which show how Q can be traded off with N (and vice versa) to achieve a given specification.

6.1. *Magnitude response: peak gain iso-N responses*

The DAPGF can be characterized by its magnitude transfer function

$$
\begin{aligned}
\left| H_{\text{DAPGF}}(j\omega) \right| &= \sqrt{H_{\text{DAPGF}}(j\omega) \times H_{\text{DAPGF}}^*(j\omega)} \\
&= \frac{\omega_o^{2N-1}\omega}{\left[\omega^4 - 2(1 - 1/2Q^2)\omega_o^2\omega^2 + \omega_o^4\right]^{N/2}}.
\end{aligned}
\tag{10}
$$

Differentiating (10) with respect to ω and setting it to zero will give the DAPGF CF $\omega_{\text{CF}}^{\text{DAPGF}}$. Fortunately, the above differentiation results in a quadratic polynomial which can be solved analytically:

$$
\frac{d\left| H_{\text{DAPGF}}(j\omega) \right|}{\omega} = 0
$$

$$
\implies \omega^4 - 2\left(\frac{N-1}{2N-1}\right)\left(1 - \frac{1}{2Q^2}\right)\omega_o^2\omega^2 - \frac{\omega_o^4}{2N-1} = 0
$$

$$
\implies \omega_{\text{CF}}^{\text{DAPGF}} = \omega_o\sqrt{\left(\frac{N-1}{2N-1}\right)\left(1 - \frac{1}{2Q^2}\right)}
$$

$$
\times \sqrt{\left(1 + \sqrt{1 + \frac{1}{\left((N-1)^2/(2N-1)\right)\left(1 - 1/2Q^2\right)^2}}\right)}.
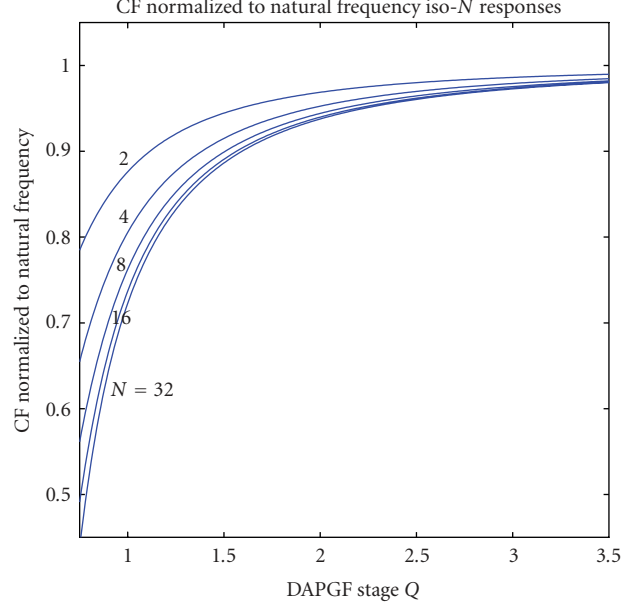\tag{11}
$$

Figure 8: DAPGF CF normalized to natural frequency iso-N responses for varying Q values. For high Q values, the behavior becomes asymptotic.

From (11), it is not exactly clear if the DAPGF has a similar behavior to the LP biquad in terms of how its CF approaches ω_o in the frequency domain as Q increases. Figure 8 shows $\omega_{\text{CF}}^{\text{DAPGF}}/\omega_o$ iso-N responses for varying Q values. Observe that as N tends to large values and (11) tends to (2), that is, for large N, the behavior is exactly that of the LP biquad (or APGF). Note that for $N = 32$ and for $Q < 1$, $\omega_{\text{CF}}^{\text{DAPGF}}/\omega_o$ is close to 0.5 (i.e., $\omega_{\text{CF}}^{\text{DAPGF}}$ is half an octave below ω_o).

Substituting (11) back to (10) will yield an expression for the peak gain. The peak gain expression was plotted in MATLAB for various N values and with Q ranging from 0.75 to 5. The result is a family of curves that can be used to determine N or Q for a fixed peak gain or vice versa. The results are shown in Figure 9. Moreover, for large N,

$$
\left| H_{\text{DAPGF}}(\omega_{\text{CF}}^{\text{DAPGF}}) \right| \approx \frac{Q^N\sqrt{1 - 1/2Q^2}}{\left[1 - 1/4Q^2\right]^{N/2}}.
\tag{12}
$$

6.2. *Bandwidth iso-N responses*

There are many acceptable definitions for the bandwidth of a filter. To be consistent with what physiologists quote, we will present Q_{10} and Q_3 as a measure of the DAPGF bandwidth. The pair of frequencies (ω_{low}, ω_{high}) for which the DAPGF gain falls $1/\gamma$ from its peak value (where γ is either $\sqrt{2}$ or $\sqrt{10}$ for 3 dB or 10 dB, resp.) are related to Q_{10} or Q_3 as follows:

$$
Q = \frac{\text{CF}}{\text{BW}} = \frac{\omega_{\text{CF}}^{\text{DAPGF}}}{\omega_{\text{high}} - \omega_{\text{low}}}.
\tag{13}
$$
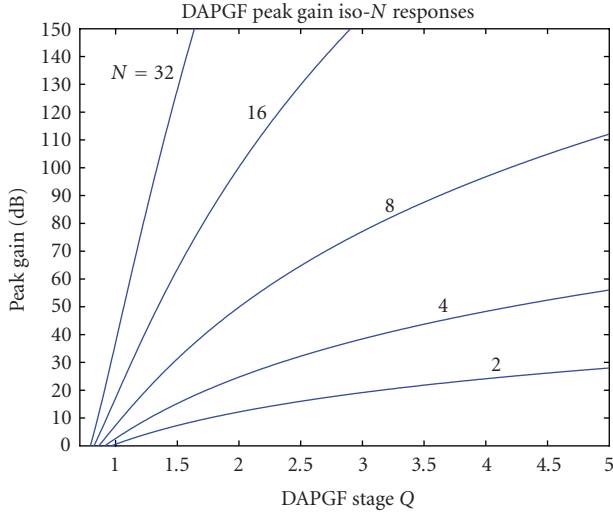
FIGURE 9: DAPGF peak gain iso-N responses for varying Q values.
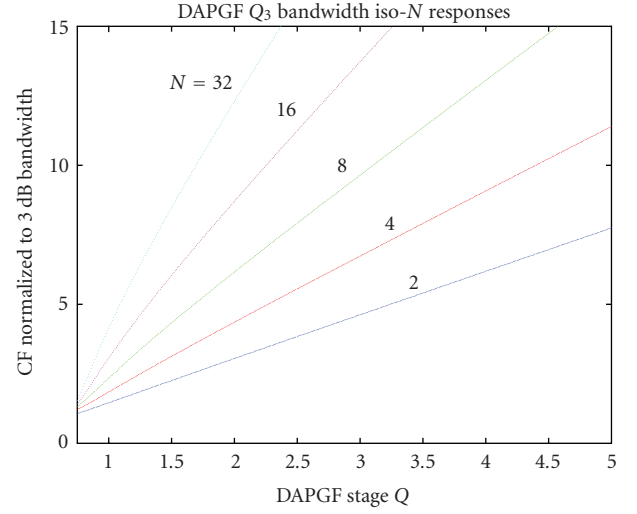
FIGURE 10: DAPGF Q_3 iso-N responses for varying Q values.

This pair of frequencies can be determined by solving the following equation:

$$
\begin{aligned}
\left| H_{\text{DAPGF}}(j\omega) \right| &= \frac{\left| H_{\text{DAPGF}}(\omega_{\text{CF}}^{\text{DAPGF}}) \right|}{\gamma} \\
\implies & \frac{\omega_o^{2N-1}\omega}{\left[\omega^4 - 2(1 - 1/2Q^2)\omega_o^2\omega^2 + \omega_o^4\right]^{N/2}} \\
&= \frac{\left| H_{\text{DAPGF}}(\omega_{\text{CF}}^{\text{DAPGF}}) \right|}{\gamma} \\
\implies & \omega\left[\omega^4 - 2\left(1 - \frac{1}{2Q^2}\right)\omega_o^2\omega^2 + \omega_o^4\right]^{-N/2} \\
&= \frac{\left| H_{\text{DAPGF}}(\omega_{\text{CF}}^{\text{DAPGF}}) \right|}{\gamma\omega_o^{2N-1}}.
\end{aligned}
\tag{14}
$$

Since (14) is raised to the power of $-N/2$, the roots of the polynomial will be different for N even and N odd. For N odd, (14) can be manipulated to yield
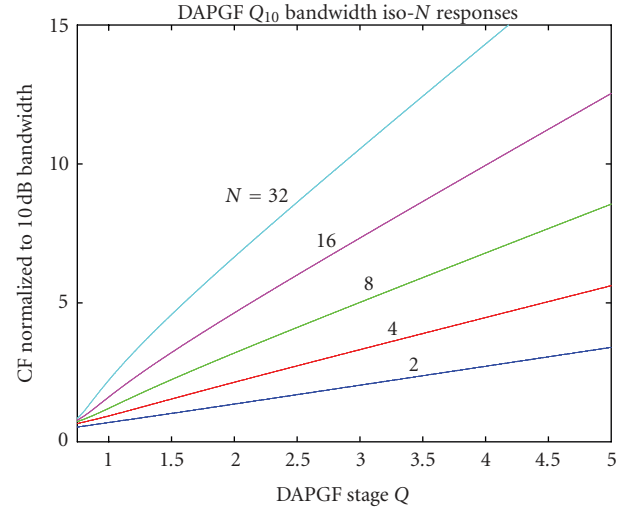
$$
\begin{aligned}
t^{2N} + & \left[-2\left(1 - \frac{1}{2Q^2}\right)\omega_o^2\right]t^N \\
& + \left[-\left(\frac{\left| H_{\text{DAPGF}}(\omega_{\text{CF}}^{\text{DAPGF}}) \right|}{\gamma\omega_o^{2N-1}}\right)^{-2/N}\right]t + \omega_o^4 = 0,
\end{aligned}
\tag{15}
$$

where $t = \omega^{2/N}$.

Similarly, for N even and $N \geq 2$,

$$
\begin{aligned}
t^{2N} + & \left[-2\left(1 - \frac{1}{2Q^2}\right)\omega_o^2\right]t^N \\
& - \left[-\left(\frac{\left| H_{\text{DAPGF}}(\omega_{\text{CF}}^{\text{DAPGF}}) \right|}{\gamma\omega_o^{2N-1}}\right)^{-2/N}\right]t + \omega_o^4 = 0,
\end{aligned}
\tag{16}
$$

where $t = \omega^{2/N}$.

FIGURE 11: DAPGF Q_{10} iso-N responses for varying Q values.

Figures 10 and 11 depict Q_3 and Q_{10} bandwidth iso-N responses for several order values with Q ranging from 0.75 to 5.

6.3. Delay and dispersion iso-N responses

Besides the magnitude, the phase of the transfer function is also of interest. The most useful view of phase is its negative derivative versus frequency, known as group delay, which is closely related to the magnitude and avoids the need for trigonometric functions. The phase response of the DAPGF is provided by

$$
\angle H_{\text{DAPGF}}(j\omega) = \frac{\pi}{2} - N \times \arctan\left(\frac{\omega_o\omega}{Q(\omega_o^2 - \omega^2)}\right).
\tag{17}
$$

The DAPGF general group delay response is obtained by differentiating (17):

$$T(\omega) = -\frac{d\angle H_{\mathrm{DAPGF}}(j\omega)}{d\omega}$$
$$= N\frac{1+x}{Q\omega_o[x^2 - 2(1 - 1/2Q^2)x + 1]}, \quad \text{where } x = (\omega/\omega_0)^2. \tag{18}$$

By normalizing the group delay relative to the natural frequency, the delay can be made nondimensional (or in terms of natural units of the system, radians at ω_o), leading to a variety of simple expressions for delay at particular frequencies:

(i) group delay at DC:

$$T(0)\omega_o = N/Q; \tag{19}$$

(ii) maximum group delay:

$$T(\omega)\omega_o = \frac{2NQ}{2 - 8Q^2\left(1 - \sqrt{1 - 1/4Q^2}\right)} \approx \frac{2NQ}{1 - 1/16Q^2}; \tag{20}$$

(iii) normalized frequency of maximum group delay:

$$\frac{\omega_{T\mathrm{peak}}}{\omega_o} = \sqrt{2\sqrt{1 - \frac{1}{4Q^2}} - 1}; \tag{21}$$

(iv) low-side dispersion.

The difference between group delay at CF and at DC is what we call the low-side dispersion, which we also normalize relative to natural frequency. This measure of dispersion is the time spread (in normalized or radian units) between the arrival of low frequencies in the tail of the DAPGF transfer function and the arrival of frequencies near CF, in response to an impulse. Figure 13 depicts low-side dispersion iso-N responses for varying N and Q:

$$(T(\omega_{\mathrm{CF}}^{\mathrm{DAPGF}}) - T(0))\omega_o$$
$$= \frac{N[1 + (\omega_{\mathrm{CF}}^{\mathrm{DAPGF}}/\omega_o)]}{Q\omega_o[(\omega_{\mathrm{CF}}^{\mathrm{DAPGF}}/\omega_o)^2 - 2(1 - 1/2Q^2)(\omega_{\mathrm{CF}}^{\mathrm{DAPGF}}/\omega_o) + 1]} + \frac{N}{Q}$$
$$\approx 2NQ\left(1 - \frac{1}{2Q^2}\right), \quad \text{for large } N. \tag{22}$$

Although many properties of BM motion are highly non-linear, in terms of traveling-wave delay, the partition behaves linearly. The actual shape of the delay function (an indicative example is shown in Figure 12) allows one to estimate the relative latency disparities between spectral components for various frequencies; the latency disparity will be very small for high frequencies <500 microseconds and considerable for lower frequencies (where the harmonics lie within the core of the spectral range of speech and music). Such latency behavior is thought to preserve the waveform of a complex stimulus when it is mechanically propagated along the cochlea partition. This situation is a necessary condition for the tempo-
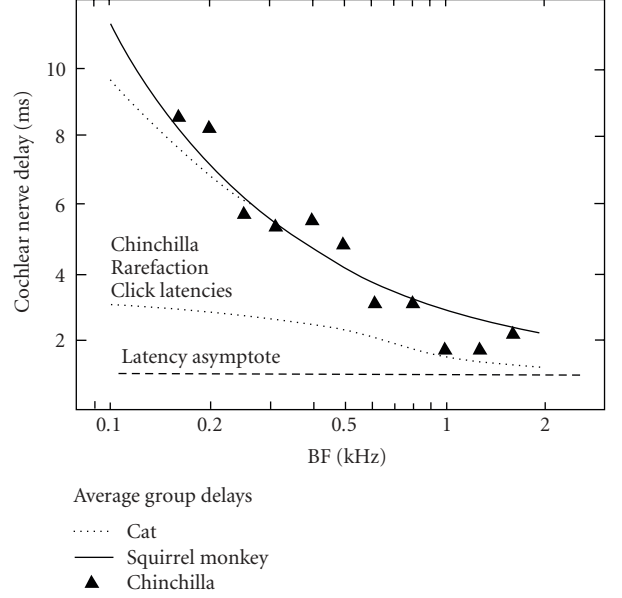

FIGURE 12: Average group delays and latencies to clicks for cochlea nerve fiber responses as a function of CF. Adapted from Ruggero and Rich (1987) [38].
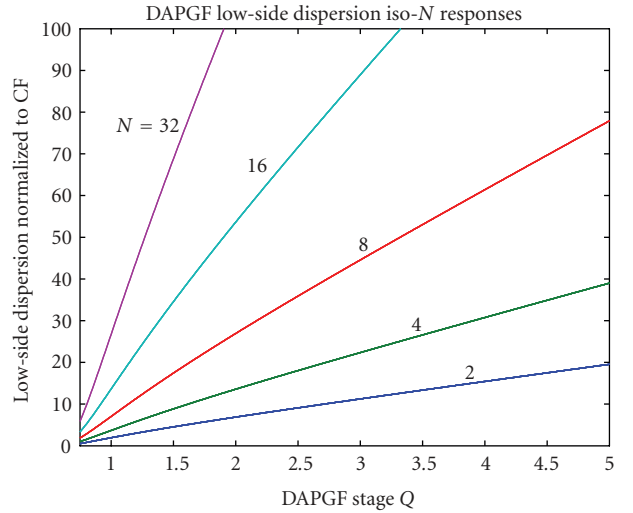

FIGURE 13: DAPGF low-side dispersion iso-N responses for varying Q values.

ral properties of the waveform to be reflected in the rhythm of neural discharges [39].

For the case of a filterbank architecture, if each channel (which maps to a different BM segment and hence at a different delay "point") has the same order N and quality factor Q, then the delays for all the channels will be the same—a much different situation from what actually happens in reality. In other words, to be able to account for delay (not just shape), each channel must be designed/modeled differently and according to delay data such as those presented in Figure 12.
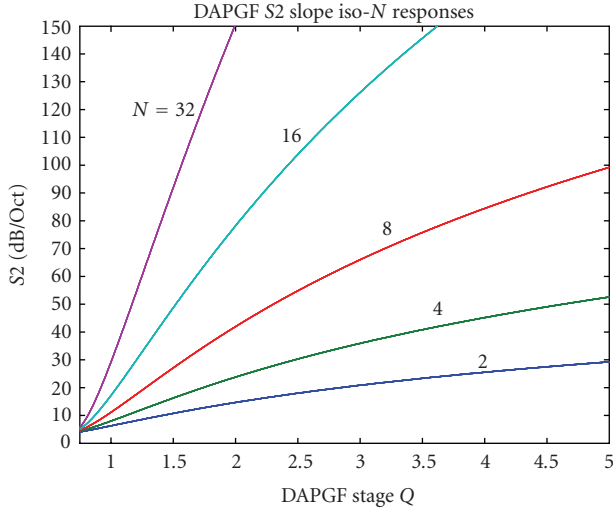
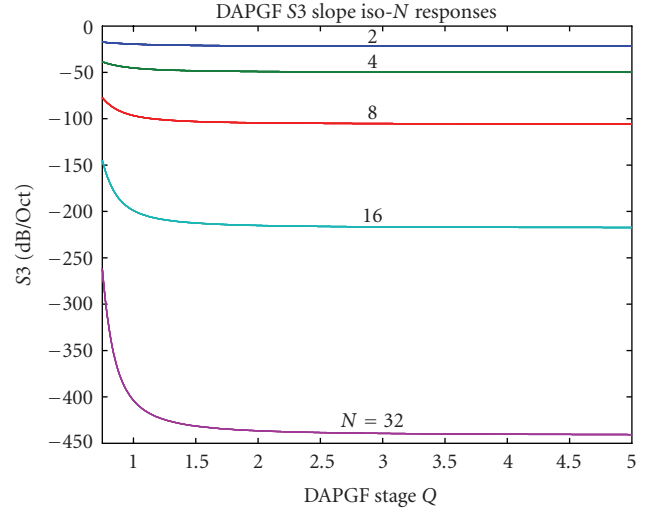FIGURE 14: DAPGF $S2$ slope iso-N responses for varying Q values.

FIGURE 15: DAPGF $S3$ slope iso-N responses for varying Q values. The $S3$ slopes are almost constant with increasing Q.

6.4.   S2 and S3 slope iso-N responses

Figure 4 and Table 1 illustrate a simple bode-plot parameterization for the BM tuning curves. In this section, we present slope iso-N responses, that is, a family of curves which shows how the slopes $S2$ and $S3$ change with varying N and Q (see Figures 14 and 15). Note that the $S3$ slope varies rather slowly with Q for each N. Thus, when trying to match a given tuning curve in terms of, say, its Q_{10} and high-frequency roll-off, it is more convenient to first fix the order which sets the $S3$ slope and then vary Q until you meet the required bandwidth value. Since the DAPGF peak gain, bandwidth, low-side dispersion, and so forth are all functions of N and Q, we can use one of the two implicitly and obtain graphs which show directly the interdependence between various DAPGF parameters. For example, Figures 16 and 17 depict low-side dispersion iso-N responses and CF relative to natural frequency iso-N, iso-Q responses as functions of the DAPGF peak gain. In this way, the engineer/modeler can directly see the order-related constraints and tradeoffs between the various parameters.

To conclude, we provide two examples of how the DAPGF can approximately be fitted to measurements from real cochleae. It should be clear by now that the bandwidth, peak gain, and slope iso-N responses are all interdependent in terms of N and Q. Thus, satisfying all simultaneously seems to be impossible for some cases. Note that for the second example, group delays were not considered.

Example 1. Using Figure 7, the first entry of Table 1 (measurements from a squirrel monkey) can be approximated by an eighth-order DAPGF with a Q of 1.44. The fitting was performed with the peak gain (28 dB) and $S3$ (-100 dB/oct) parameters in mind. Now, assume that one needs to build a 7-channel filterbank with the delays per channel varying according to the solid-line plot of Figure 12. Also, assume that we are interested in the peak gain parameter with all channels having the potential to achieve equal peak gains of no more
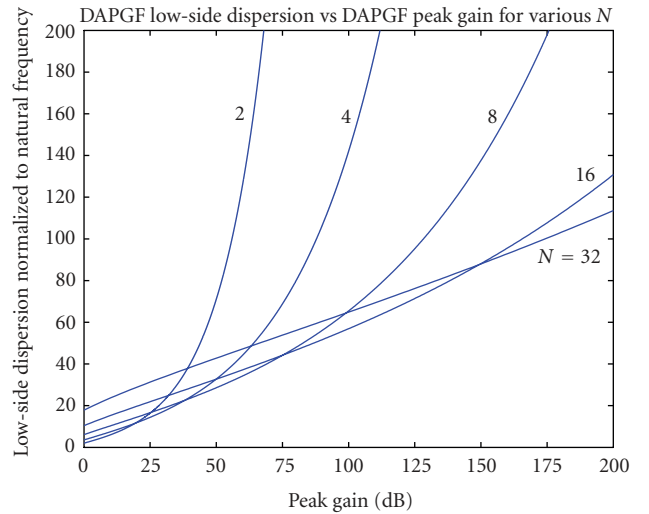

FIGURE 16: DAPGF low-side dispersion versus peak gain for various N. The behavior for high N is not asymptotic; rather, the total dispersion continues to increase with N once N is high enough for the particular peak gain value.

than 28 dB with small-to-moderate Q values. Using (20) and the general equation for the peak gain, a set of graphs of maximum group delay iso-N, iso-Q responses as a function of the DAPGF peak gain can be obtained. Figure 18 depicts these results, whereas the per-channel parameters are tabulated in Table 3.

Example 2. Robles et al. in [40] present measurements from very sensitive tuning curves at the base of the chinchilla cochlea. One of their measurements resulted in a tuning curve with a Q_{10} of 5.3 and an $S3$ slope of -270 dB/oct. Using Figures 11 and 15, this can be reasonably approximated by a DAPGF of $N = 20$ and $Q = 2.028$ (specifically for these N and Q, the DAPGF equations give $Q_{10} = 5.3002$ and $S3 = -270.5856$ dB/oct). Their most sensitive animal gave a
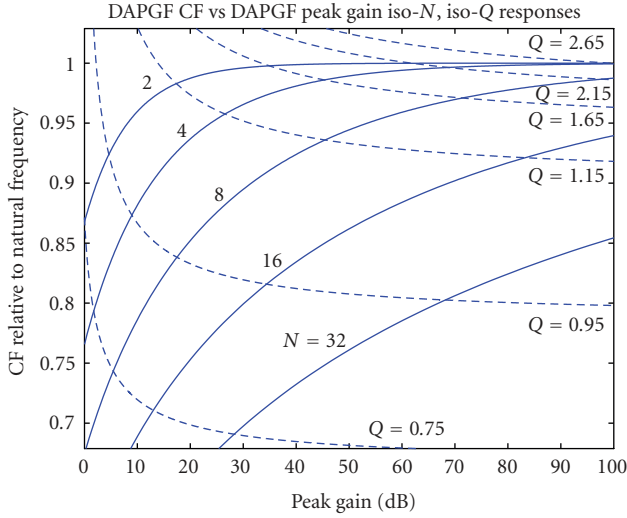
DAPGF CF vs DAPGF peak gain iso-N, iso-Q responses

FIGURE 17: DAPGF CF versus peak gain for several values of N, illustrating a range of possible dependencies of CF on gain, and hence indirectly on level, under the assumption of constant natural frequency. Indicative iso-Q responses are superimposed on the plot.

DAPGF maximum group delay iso-N, iso-Q responses

FIGURE 18: DAPGF maximum group delay versus peak gain for several values of N, illustrating a range of possible dependencies of delay on gain, and hence indirectly on level, under the assumption of constant natural frequency. Indicative iso-Q responses are superimposed on the plot. The order increases linearly from 2 to 32 in increments of 2. Note also that not all delay values can be related to a particular peak gain value.

Q_{10} of 6.1 and an $S3$ slope of -313 dB/oct; this can be approximated by a DAPGF of $N = 23$ and $Q = 2.2$.

6.5. Asymmetry from symmetry

One of the most striking features of auditory tuning curves is the asymmetry between the low-frequency and high-

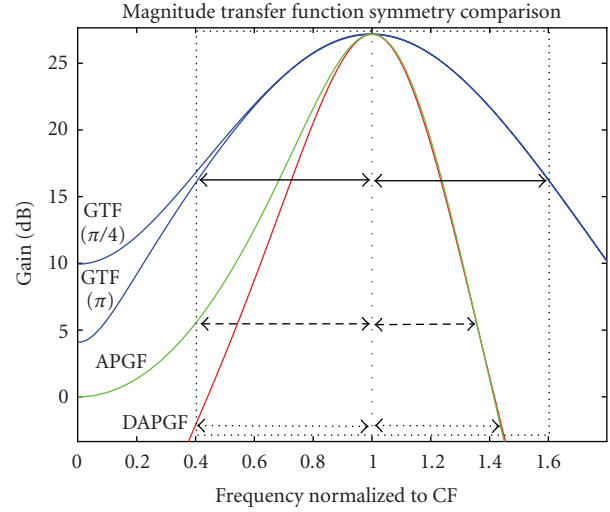Magnitude transfer function symmetry comparison

FIGURE 19: Comparison of magnitude transfer functions of the nearly symmetric GTF and the clearly asymmetric APGF and DAPGF, on a linear frequency scale normalized to CF. The peak gains and CFs for all filters were adjusted to coincide exactly.
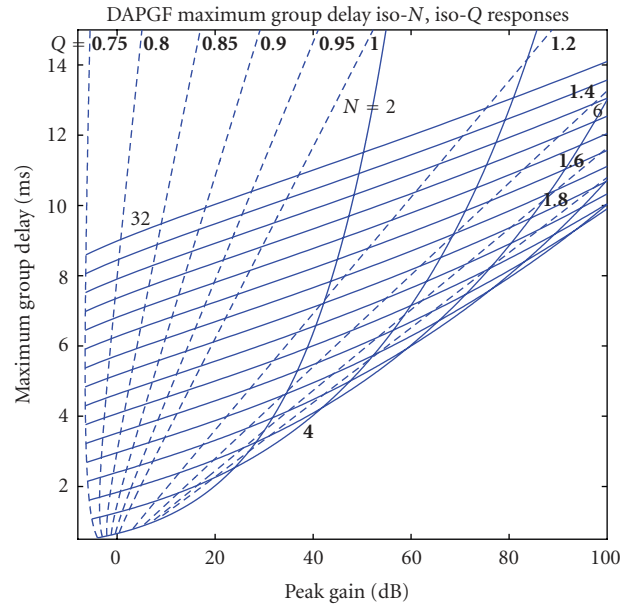
TABLE 3: Approximate 7-channel filterbank parameters for example 1.

Delay (ms)	N	$\sim Q$	$\sim$CF (kHz)
3	5	1.86	1
4	9	1.35	0.5
5	13	1.18	0.38
6	16	1.11	0.27
7	20	1.05	0.2
8	24	1.005	0.18
9	27	0.983	0.15

frequency "tails" or "skirts." In addition, the degree of asymmetry is known to vary with signal level. Patterson et al. [41] observed that "the gammatone filter has one notable disadvantage: the amplitude characteristic is virtually symmetric for orders equal to or greater than two, and there is no obvious way to introduce asymmetry." Figure 19 shows a comparison between the GTF (two phases: π and $\pi/4$), APGF, and DAPGF in terms of their asymmetry in the passband. For the GTF, varying its phase parameter can make its response more asymmetric in either direction, but only by very little as Patterson and Nimmo-Smith observed in [42]. Varying its bandwidth parameter has a similarly small and nonmonotonic effect on the asymmetry. In either case, the greatest relative variation occurs in the low-frequency tail of the GTF response.

The APGF and DAPGF (and hence OZGF) exhibit a kind of asymmetry that is comparable to physiological data. Moreover, the degree of asymmetry, observed within a limited range, for example, within 30 dB of the peak, is a strong function of Q and as such it can be associated with level. For the APGF, DAPGF, and OZGF, the level dependence of
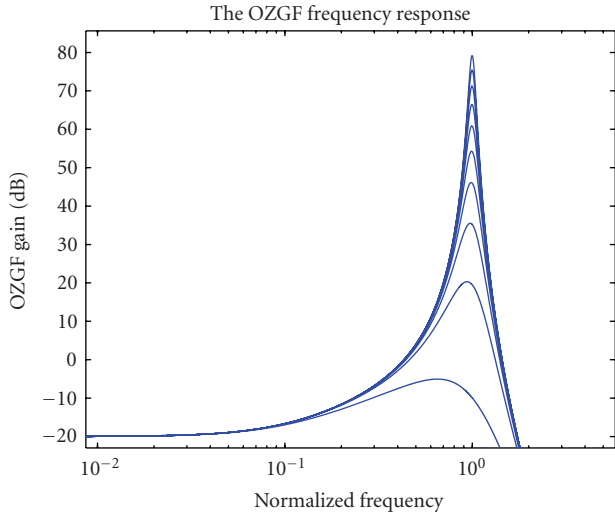
FIGURE 20: The OZGF frequency response of order 4 with Q ranging from 0.75 to 10. The zero was placed at a frequency of 1/10 of the natural frequency. The frequency axis is normalized to the natural frequency.
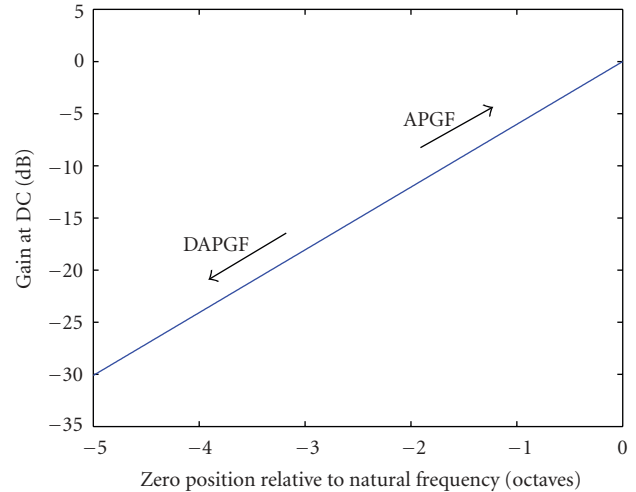

FIGURE 21: OZGF DC gain versus zero position relative to natural frequency. Observe that if the zero is placed at 3.32 octaves (i.e., one decade) below the natural frequency, the DC level of the low-frequency tail is at -20 dB. The DC gain is independent of Q and the order N.

gain, bandwidth, and frequency-domain asymmetry are all correctly coupled via Q variation.

As a last remark, it is important to note that the asymmetric APGF, DAPGF, and OZGF responses are all derived by discarding all or all but one of the zeros from the nearly symmetric GTF. In other words, asymmetry seems to be inversely proportional to the number of zeros appearing in the transfer function.

7. OBSERVATIONS ON THE OZGF RESPONSE

Referring back to Figure 2, one may observe that the low-frequency tail of the response has a gain value at DC of 10^{-1}, which translates to -20 dB. By setting in (7) (see Table 2) the frequency of the zero to be one decade lower than the natural frequency, that is, $\omega_z = 0.1\omega_o$, we obtain the response of the OZGF shown in Figure 20. The OZGF can be considered as a GTF variant that lies in the continuum between DAPGF and APGF. Its zero is not fixed at DC; rather it can be set to any real nonzero value. The OZGF is a more realistic model of the BM tuning curves than the DAPGF and can be used to fit more accurately experimental physiological data.

The parameters' peak gain, bandwidth, low-side dispersion remain nearly unaffected by the tuning of this zero; the only parameter that changes is the DC level of the low-frequency tail. From the implementation point of view, the OZGF may be viewed as a cascade of $(N-1)$ identical LP biquads together with a lossy BP biquad (i.e., a 2-pole, 1-zero transfer function), which is easier to design than a pure BP response due to its DC stability.

Figure 21 shows a plot of the OZGF DC gain as a function of the zero position relative to the natural frequency. It should be stressed that the closer this zero is to the natural frequency, the closer the OZGF response approaches that of an APGF, and its peak gain, bandwidth, low-side dispersion,

and so forth acquire slightly different values. Conversely, the further away it is from the natural frequency, the closer the OZGF response approaches that of a DAPGF. For example, in Figure 22, we show the OZGF response of order 4 with a Q of 10 for various zero positions. As the zero moves away from the natural frequency, the peak gain gets closer and closer to the value obtained for the DAPGF (i.e., ~ 80 dB). The conclusion is that all the parameterized figures presented so far can be used for the case of the OZGF with an accuracy of better than 1 dB if the zero is placed at a reasonable distance away from the natural frequency.

8. FURTHER DISCUSSION AND CONCLUSION

This paper dealt with continuous-time filter transfer functions which closely resemble the responses obtained from BM measurements of the mammalian cochleae. The transfer functions, namely, the DAPGF and OZGF, are derived from the GTF which is a widely accepted auditory filter for modeling a variety of cochlea frequency-domain phenomena. Yet, its frequency-domain complexity and the behavior of its "spurious" zeros in particular make the association of certain attributes of the GTF with level a quite difficult one.[2] In addition, the GTF is nearly symmetric while physiological measurements show a significant asymmetry in the cochlea transfer functions. From the practical realization point of view, even though digital implementations of the GTF response have been reported, for example, [44–46], realizing the GTF in the analog domain (for the implementation of low-power, high-dynamic range, custom analog VLSI audio processors) seems to be a rather complicated task.

_____

[2] Recently, an architecture—called the dual-resonance nonlinear (DRNL) filter—that incorporates level control to the GTF was reported in [43].
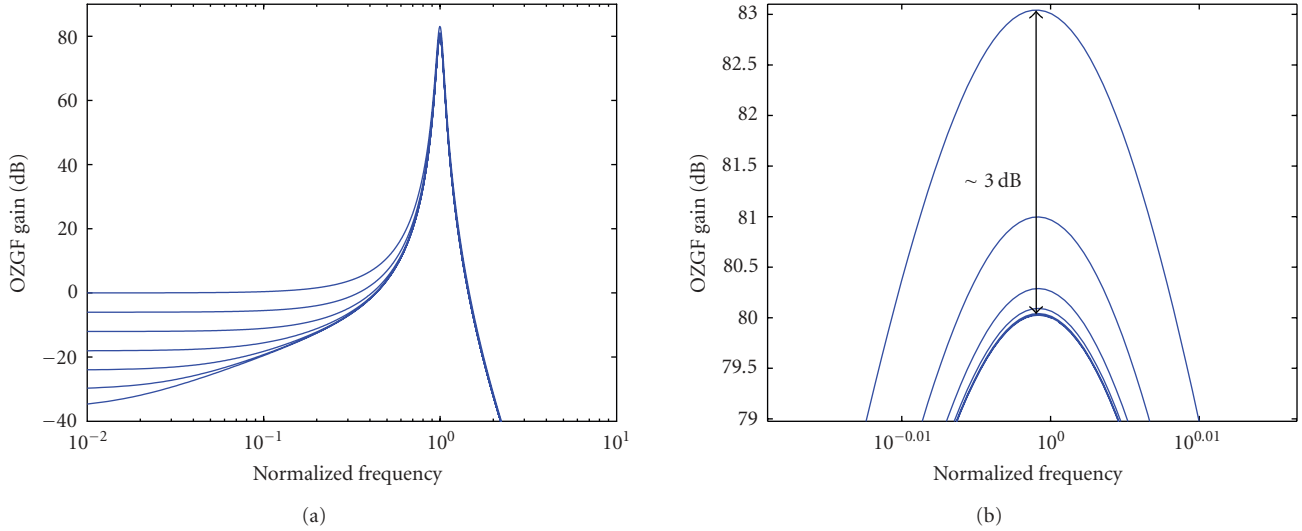
FIGURE 22: The OZGF frequency response of order 4 with a Q of 10. The zero position was varied from 0 to 5 octaves away from the natural frequency. Within that range, the peak gain changed only by 3 dB. The frequency axis is normalized to the natural frequency.

The parameterization presented in this paper, as well as the iso-N (and iso-Q) responses, provides the engineer/modeler with practical tools for designing transfer functions that meet certain performance/modeling criteria regarding peak gain, selectivity, asymmetry, delay, and so forth. The choice of using the frequency domain as opposed to time for fitting to physiological cochlea responses was made due to (a) the relative easiness to visualize with (and therefore directly link to) VLSI-compatible structures, (b) the fact that the majority of physiological measurements reported are presented in frequency-domain format, and (c) the fact that measurements recorded from an engineered (artificial) cochlea system are facilitated by a variety of frequency-domain pieces of instrumentation. For a thorough review and summary of many measurements from various sources, the reader is referred to [47].

It is understood that DAPGF and OZGF are not the most accurate responses for fitting to physiological measurements (polynomial fitting, e.g., as in [9, 48], will be much more precise), but they are implementable in hardware and in any technology while grasping most of the real cochlea's frequency-domain behavior.

In addition, it is important to appreciate that there is no such thing as a "winning" or "most suitable" DAPGF/OZGF response. In other words, there is no DAPGF/OZGF of a given N and a given Q that can meet most physiological/modeling demands. The "winner" is eventually technology-, application-, and specification-restricted. That is why we deliberately avoided presenting a "design recipe" for fitting to physiological data.

For example, one of our most recent engineering efforts details the design of an analog VLSI implementation of a fourth-order OZGF channel for real-time cochlea processing. The channel (together with its AGC mechanism) was designed in $0.35\,\mu$m AMS CMOS process using class-AB pseudodifferential log-domain biquads [49]. The partic-

ular closed-loop system achieves a simulated input dynamic range of 120 dB while dissipating $4\,\mu$W of power—figures somewhat comparable to the ones obtained from the real cochlea. The overall structure is pseudodifferential (this is a design/architecture constraint), which means that in order to realize a single pole, one needs two integrating capacitors. In other words, for a fourth-order OZGF channel (i.e., an eighth-order cascaded filter structure), one would need 16 capacitors. That is a considerable chip area requirement, especially when designing in low frequencies (large capacitors). Moreover, for filterbank applications, one needs many such channels, each tuned at a slightly different frequency.

The above example illustrates that the "winner" eventually will be the one that will meet not only the specifications presented by the physiologists, modelers, or engineers, but also the prescribed budget. Also, there are certain technological boundaries that forbid the design of very-high-Q, very-high-N OZGF channels (like instability and noise and/or DC offsets propagation and accumulation). In addition, there are many circuit design techniques that can be used to realize these transfer functions in analog VLSI with each one leading to different topologies and with most probably different constraints and optimization tradeoffs. If we consider these application- and technology-oriented factors as well, the "who-is-the-winner" query becomes a multiparametric optimization process. In digital (or software) implementations, the situation is much different. In principle, the designer/modeler can use as big an order and as big a quality factor as he needs to meet certain physiological-related specifications.

The emphatic conclusion is that the *asymmetric* DAPGF and OZGF responses seem to be very promising alternatives to the GTF. Their ability to model filter gain, not just shape, will unify the modeling of compressive gain control and filter shape as a function of signal level. Their analytical description and characterization in this paper together with

the simplicity to synthesize (cascades of biquadratic sections) render them as the ideal candidates for efficient analog or digital VLSI implementations. Many applications in which the GTF has been successful will be unaffected by changing to DAPGF or OZGF. But the DAPGF or OZGF will provide a significant benefit in applications that need a better model of level dependence or a better low-frequency tail behavior.

ACKNOWLEDGMENTS

REFERENCES

[1] C. Mead, "Neuromorphic electronic systems," *Proceedings of the IEEE*, vol. 78, no. 10, pp. 1629–1636, 1990.

[2] R. F. Lyon and C. A. Mead, "A CMOS VLSI cochlea," in *Proceedings of IEEE International Conference on Acoustics, Speech and Signal Processing (ICASSP '88)*, pp. 2172–2175, New York, NY, USA, April 1988.

[3] R. Sarpeshkar, R. F. Lyon, and C. A. Mead, "An analog VLSI cochlea with new transconductance amplifiers and nonlinear gain control," in *Proceedings of IEEE International Symposium on Circuits and Systems (ISCAS '96)*, vol. 3, pp. 292–295, Atlanta, Ga, USA, May 1996.

[4] L. Watts, D. A. Kerns, R. F. Lyon, and C. A. Mead, "Improved implementation of the silicon cochlea," *IEEE Journal of Solid-State Circuits*, vol. 27, no. 5, pp. 692–700, 1992.

[5] J. Georgiou and C. Toumazou, "A 126-μW cochlear chip for a totally implantable system," *IEEE Journal of Solid-State Circuits*, vol. 40, no. 2, pp. 430–443, 2005.

[6] Y. Kuraishi, K. Nakayama, K. Miyadera, and T. Okamura, "A single-chip 20-channel speech spectrum analyzer using a multiplexed switched-capacitor filter bank," *IEEE Journal of Solid-State Circuits*, vol. 19, no. 6, pp. 964–970, 1984.

[7] R. F. Lyon, "Cost, power, and parallelism in speech signal processing," in *Proceedings of the IEEE Custom Integrated Circuits Conference (CICC '93)*, pp. 1–10, San Diego, Calif, USA, May 1993.

[8] R. Sarpeshkar, "Brain power: borrowing from biology makes for low-power computing," *IEEE Spectrum*, vol. 43, no. 5, pp. 24–29, 2006.

[9] L. Lin, E. Ambikairajah, and W. H. Holmes, "Log-magnitude modelling of auditory tuning curves," in *Proceedings of IEEE International Conference on Acoustics, Speech and Signal Processing (ICASSP '01)*, vol. 5, pp. 3293–3296, Salt Lake, Utah, USA, May 2001.

[10] E. M. Drakakis and A. J. Payne, "On the exact realization of LC ladder finite transmission zeros in log-domain: a theoretical study," in *Proceedings of IEEE International Symposium on Circuits and Systems (ISCAS '00)*, vol. 1, pp. 188–191, Geneva, Switzerland, May 2000.

[11] T. Gold, "Hearing. II. The physical basis of the action of the cochlea," *Proceedings of the Royal Society of London. Series B*, vol. 135, no. 881, pp. 492–498, 1948.

[12] T. Gold and R. J. Pumphrey, "Hearing. I. The cochlea as a frequency analyzer," *Proceedings of the Royal Society of London. Series B*, vol. 135, no. 881, pp. 462–491, 1948.

[13] H. Helmholtz, *On the Sensations of Tone as a Physiological Basis for the Theory of Music*, Longmans, London, UK, 1885.

[14] G. von Békésy, *Experiments in Hearing*, McGraw-Hill, New York, NY, USA, 1960.

[15] D. T. Kemp, "Evidence of mechanical nonlinearity and frequency selective wave amplification in the cochlea," *European Archives of Oto-Rhino-Laryngology*, vol. 224, no. 1-2, pp. 37–45, 1979.

[16] J. C. Steinberg and M. B. Gardner, "The dependence of hearing impairment on sound intensity," *Journal of the Acoustical Society of America*, vol. 9, no. 1, pp. 11–23, 1937.

[17] W. S. Rhode, "Observations of the vibration of the basilar membrane in squirrel monkeys using the Mossbauer technique," *Journal of the Acoustical Society of America*, vol. 49, no. 4, pp. 1218–1231, 1971.

[18] W. S. Rhode and A. Recio, "Study of mechanical motions in the basal region of the chinchilla cochlea," *Journal of the Acoustical Society of America*, vol. 107, no. 6, pp. 3317–3332, 2000.

[19] M. A. Ruggero, S. S. Narayan, A. N. Temchin, and A. Recio, "Mechanical bases of frequency tuning and neural excitation at the base of the cochlea: comparison of basilar-membrane vibrations and auditory-nerve-fiber responses in chinchilla," *Proceedings of the National Academy of Sciences of the United States of America*, vol. 97, no. 22, pp. 11744–11750, 2000.

[20] W. S. Rhode, "Some observations on cochlear mechanics," *Journal of the Acoustical Society of America*, vol. 64, no. 1, pp. 158–176, 1978.

[21] J. Allen, "Nonlinear cochlear signal processing," in *Physiology of the Ear*, pp. 393–442, Singular Thompson, San Diego, Calif, USA, 2nd edition, 2001.

[22] S. S. Narayan and M. A. Ruggero, "Basilar-membrane mechanics at the hook region of the chinchilla cochlea," *Mechanics of Hearing*, 2000.

[23] M. A. Ruggero, N. C. Rich, A. Recio, S. S. Narayan, and L. Robles, "Basilar-membrane responses to tones at the base of the chinchilla cochlea," *Journal of the Acoustical Society of America*, vol. 101, no. 4, pp. 2151–2163, 1997.

[24] J. B. Allen, "Magnitude and phase-frequency response to single tones in the auditory nerve," *Journal of the Acoustical Society of America*, vol. 73, no. 6, pp. 2071–2092, 1983.

[25] P. I. M. Johannesma, "The pre-response stimulus ensemble of neuron in the cochlear nucleus," in *Proceedings of the Symposium of Hearing Theory*, Eindhoven, The Netherlands, 1972.

[26] L. H. Carney and T. C. T. Yin, "Temporal coding of resonances by low-frequency auditory nerve fibers: single-fiber responses and a population model," *Journal of Neurophysiology*, vol. 60, no. 5, pp. 1653–1677, 1988.

[27] E. de Boer and H. R. de Jongh, "On cochlear encoding: potentialities and limitations of the reverse-correlation technique," *Journal of the Acoustical Society of America*, vol. 63, no. 1, pp. 115–135, 1978.

[28] J. L. Flanagan, "Models for approximating basilar membrane displacement," *Journal of the Acoustical Society of America*, vol. 32, no. 7, p. 937, 1960.

[29] A. M. H. J. Aertsen and P. I. M. Johannesma, "Spectro-temporal receptive fields of auditory neurons in the grassfrog—I: characterization of tonal and natural stimuli," *Biological Cybernetics*, vol. 38, no. 4, pp. 223–234, 1980.

[30] J. L. Flanagan, "Models for approximating basilar membrane displacement—II: effects of middle-ear transmission," *Journal of the Acoustical Society of America*, vol. 32, no. 11, pp. 1494–1495, 1960.

[31] R. D. Patterson, "The sound of a sinusoid: spectral models," *Journal of the Acoustical Society of America*, vol. 96, no. 3, pp. 1409–1418, 1994.

[32] P. F. Assmann and Q. Summerfield, "Modeling the perception of concurrent vowels: vowels with the same fundamental frequency," *Journal of the Acoustical Society of America*, vol. 85, no. 1, pp. 327–338, 1989.

[33] R. Meddis and M. J. Hewitt, "Virtual pitch and phase sensitivity of a computer model of the auditory periphery. I: pitch identification," *Journal of the Acoustical Society of America*, vol. 89, no. 6, pp. 2866–2882, 1991.

[34] M. Holmes and J. D. Cole, "Pseudoresonance in the cochlea," in *Mechanics of Hearing*, E. deBoer and M. A. Viergever, Eds., Martinus Nijhoff, Hague, The Netherlands, 1983.

[35] R. F. Lyon, "The all-pole gammatone filter and auditory models," *Acustica*, vol. 82, p. S90, 1996.

[36] M. Slaney, "An efficient implementation of the Patterson-Holdsworth auditory filter bank," Tech. Rep. #35, Apple Computer, Cupertino, Calif, USA, 1993.

[37] A. Recio, N. C. Rich, S. S. Narayan, and M. A. Ruggero, "Basilar-membrane responses to clicks at the base of the chinchilla cochlea," *Journal of the Acoustical Society of America*, vol. 103, no. 4, pp. 1972–1989, 1998.

[38] M. A. Ruggero and N. C. Rich, "Timing of spike initiation in cochlear afferents: dependence on site of innervation," *Journal of Neurophysiology*, vol. 58, no. 2, pp. 379–403, 1987.

[39] J. F. Brugge, D. J. Anderson, J. E. Hind, and J. E. Rose, "Time structure of discharges in single auditory nerve fibers of the squirrel monkey in response to complex periodic sounds," *Journal of Neurophysiology*, vol. 32, no. 3, pp. 386–401, 1969.

[40] M. A. Ruggero, L. Robles, and N. C. Rich, "Basilar membrane mechanics at the base of the chinchilla cochlea—II: response to low-frequency tones and relationship to microphonics and spike initiation in the VIII nerve," *Journal of the Acoustical Society of America*, vol. 80, no. 5, pp. 1375–1383, 1986.

[41] R. D. Patterson, I. Nimmo-Smith, J. Holdsworth, and P. Rice, "Spiral VOS final report—part A: the auditory filterbank," Internal Report 2341, MRC Applied Psychology Unit, Cambridge, UK, 1988.

[42] R. D. Patterson and I. Nimmo-Smith, "Off-frequency listening and auditory-filter asymmetry," *Journal of the Acoustical Society of America*, vol. 67, no. 1, pp. 229–245, 1980.

[43] E. A. Lopez-Poveda, "A human nonlinear cochlear filterbank," *Journal of the Acoustical Society of America*, vol. 110, no. 6, pp. 3107–3118, 2001.

[44] L. van Immerseel and S. Peeters, "Digital implementation of linear gammatone filters: comparison of design methods," *Acoustic Research Letters Online*, vol. 4, pp. 59–64, 2003.

[45] P. R. Dorrell and P. N. Denbigh, "Spectrograms of overlapping speech based upon instantaneous frequency," in *Proceedings of International Symposium on Speech, Image Processing and Neural Networks (ISSIPNN '94)*, pp. 607–610, Hong Kong, April 1994.

[46] L. Lin, W. H. Holmes, and E. Ambikairajah, "Auditory filter bank inversion," in *Proceedings of IEEE International Symposium on Circuits and Systems (ISCAS '01)*, vol. 2, pp. 537–540, Sydney, Australia, May 2001.

[47] L. Robles and M. A. Ruggero, "Mechanics of the mammalian cochlea," *Physiological Reviews*, vol. 81, no. 3, pp. 1305–1352, 2001.

[48] S. Rosen, R. J. Baker, and A. Darling, "Auditory filter nonlinearity at 2 kHz in normal hearing listeners," *Journal of the Acoustical Society of America*, vol. 103, no. 5 I, pp. 2539–2550, 1998.

[49] A. G. Katsiamis, E. Drakakis, and R. F. Lyon, "Introducing the differentiated all-pole and one-zero gammatone filter responses and their analogue VLSI log-domain implementation," in *Proceedings of the 49th International Midwest Symposium on Circuits and Systems (MWSCAS '06)*, pp. 561–565, San Juan, Puerto Rico, USA, August 2006.

Special Issue on
Network Structure and Biological Function: Reconstruction, Modelling, and Statistical Approaches

Call for Papers

We are particularly interested in contributions, which elucidate the relationship between structure or dynamics of biological networks and biological function. This relationship may be observed on different scales, for example, on a global scale, or on the level of subnetworks or motifs.

Several levels exist on which to relate biological function to network structure. Given molecular biological interactions, networks may be analysed with respect to their structural and dynamical patterns, which are associated with phenotypes of interest. On the other hand, experimental profiles (e.g., time series, disturbances) can be used to reverse engineer network structures based on a model of the underlying functional network.

Is it possible to detect the interesting features with the current methods? And how is our picture of the relationsship between network structure and biological function affected by the choice of methods?

Perspectives both from simulation approaches as well as the evaluation of experimental data and combinations thereof are welcome and will be integrated within this special issue.

Authors should follow the EURASIP Journal on Bioinformatics and Systems Biology manuscript format described at the journal site http://www.hindawi.com/journals/bsb/. Prospective authors should submit an electronic copy of their complete manuscript through the journal Manuscript Tracking System at http://mts.hindawi.com/, according to the following timetable:

Manuscript Due	June 1, 2008
First Round of Reviews	September 1, 2008
Publication Date	December 1, 2008

D. Repsilber, AG Biomathematics & Bioinformatics, Genetics and Biometry and Genetics Section, Research Institute for the Biology of Farm Animals, Dummerstorf, Germany; repsilber@fbn-dummerstorf.de

Guest Editors

J. Selbig, Bioinformatics Chair, Institute for Biochemistry and Biology, University of Potsdam, Germany; selbig@mpimp-golm.mpg.de

M. Steinfath, Institute for Biochemistry and Biology, University of Potsdam, Germany; steinfath@mpimp-golm.mpg.de

RESEARCH LETTERS IN
SIGNAL PROCESSING

Why publish in this journal?

Research Letters in Signal Processing is devoted to very fast publication of short, high-quality manuscripts in the broad field of signal processing. Manuscripts should not exceed 4 pages in their final published form. Average time from submission to publication shall be around 60 days.

Why publish in this journal?

Wide Dissemination

All articles published in the journal are freely available online with no subscription or registration barriers. Every interested reader can download, print, read, and cite your article.

Quick Publication

The journal employs an online "Manuscript Tracking System" which helps streamline and speed the peer review so all manuscripts receive fast and rigorous peer review. Accepted articles appear online as soon as they are accepted, and shortly after, the final published version is released online following a thorough in-house production process.

Professional Publishing Services

The journal provides professional copyediting, typesetting, graphics, editing, and reference validation to all accepted manuscripts.

Keeping Your Copyright

Authors retain the copyright of their manuscript, which is published using the "Creative Commons Attribution License," which permits unrestricted use of all published material provided that it is properly cited.
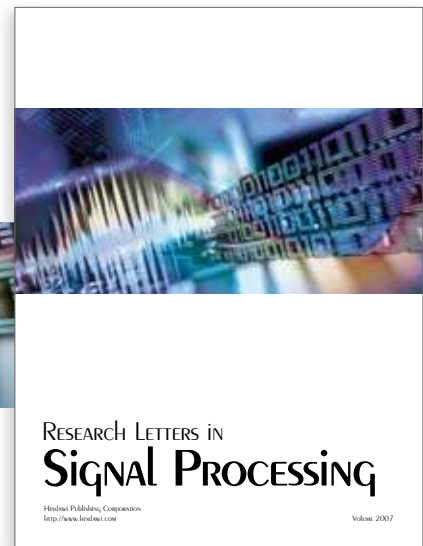
Extensive Indexing

Articles published in this journal will be indexed in several major indexing databases to ensure the maximum possible visibility of each published article.

Submit your Manuscript Now...

In order to submit your manuscript, please visit the journal's website that can be found at **http://www.hindawi.com/journals/rlsp/** and click on the "Manuscript Submission" link in the navigational bar.

Should you need help or have any questions, please drop an email to the journal's editorial office at **rlsp@hindawi.com**